Enhancement of Terahertz Pulse Emission by Optical Nanoantenna

Sang-Gil Park,[†,§] Kyong Hwan Jin,[†] Minwoo Yi,[‡,§] Jong Chul Ye,[†] Jaewook Ahn,[‡,§] and Ki-Hun Jeong[†,§,*]

[†]Department of Bio and Brain Engineering, [‡]Department of Physics, and [§]KAIST Institute for Optical Science and Technology, Korea Advanced Institute of Science and Technology (KAIST), 291 Daehak-ro, Yuseong-gu, Daejeon 305-701, Republic of Korea

ABSTRACT

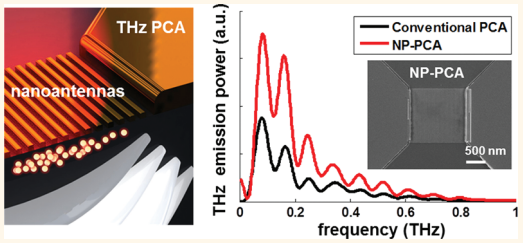

Bridging the gap between ultrashort pulsed optical waves and terahertz (THz) waves, the THz photoconductive antenna (PCA) is a major constituent for the emission or detection of THz waves by diverse optical and electrical methods. However, THz PCA still lacks employment of advanced breakthrough technologies for high-power THz emission. Here, we report the enhancement of THz emission power by incorporating optical nanoantennas with a THz photoconductive antenna. The confinement and concentration of an optical pump beam on a photoconductive substrate can be efficiently achieved with optical nanoantennas over a high-index photoconductive substrate. Both numerical and experimental results clearly demonstrate the enhancement of THz wave emission due to high photocarrier generation at the plasmon resonance of nanoantennas. This work opens up many opportunities for diverse integrated photonic elements on a single PCA at THz and optical frequencies.

KEYWORDS: nanoplasmonics · optical nanoantenna · THz photoconductive antenna · plasmon resonance · THz emission power

For the past few decades, THz technology has been extensively developed to bridge between microwave and optical frequency.[1−5] THz time domain spectroscopy can provide unique spectral molecular fingerprints in many biological applications, such as label-free biomolecular analysis,[6] polymorph classification,[7] or skin cancer diagnosis.[8,9] Unlike other THz pulse emitters, a THz photoconductive antenna (PCA) can offer relatively high power emission as a standard THz pulse emitter.[10] In PCA-based THz pulse emission, femtosecond optical pulses with photon energy higher than the band gap impinge onto a photoconductive substrate, and they generate the photon-induced charge carriers. Accelerated by the bias electric field between the PCA electrodes, the excited photocarriers induce the transient photocurrent and the electromagnetic waves at THz frequencies.

Nano- and microfabrication can provide many opportunities for increasing the emission power of THz PCA. Previous works have been reported for planar large-area PCA arrays by employing interdigitized microelectrodes to produce constructive interference of THz waves, and more recently, microlens arrays have been integrated to focus an optical pump beam on the PCA arrays for high-power THz generation.[11−14] However, the previous works still require a high-power femtosecond pulse laser over the large area.

Nanoplasmonics is a state-of-the-art candidate for more actively interacting photons with matter.[15,16] Recently, the unique properties of metal nanostructures have been intensively explored as an optical nanoantenna.[17−19] The optical nanoantennas offer both strong light concentration in the near-field and light confinement into a high-index substrate. The strong light concentration, that is, the locally enhanced electric field, can efficiently occur at the localized surface plasmon resonance (LSPR) of optical nanoantennas, and the intense light confinement can also be achieved by asymmetric scattering due to surface plasmon excited on metal nanostructures.[15] The optical nanoantennas have been actively applied for enhancing the conversion efficiency of photon-to-electron conversion for photodetectors,[20−22] light-emitting diodes,[23] and photovoltaic devices[15,24−28] due to high photocarrier generation in a photoconductive layer.

This work reports the enhancement of THz pulse emission power from a photoconductive antenna with optical nanoantenna arrays, that is, nanoplasmonic PCA (NP-PCA). The device features gold nanorod arrays between two microelectrodes on a

* Address correspondence to kjeong@kaist.ac.kr.

Received for review August 25, 2011 and accepted February 17, 2012.

Published online February 17, 2012
10.1021/nn204542x

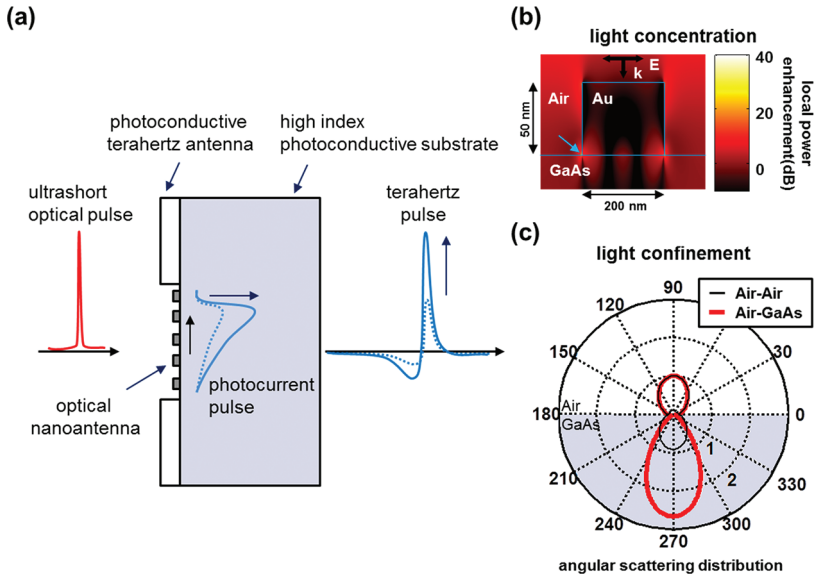

Figure 1. Enhancement of terahertz emission power from a photoconductive antenna with optical nanoantenna arrays. (a) Optical nanoantennas increase photocurrent on a high-index photoconductive substrate due to light concentration and asymmetric light scattering. THz emission power is then enhanced by the increase of transient photocurrent. (b) Light concentration due to the nanoantenna at an excitation wavelength. The local powers of the optical pump beam are enhanced 130-fold in maximum (arrowed) and 2.4-fold on average at the interface. (c) Light confinement due to asymmetric angular scattering distribution by the nanoantenna at excitation wavelength. Asymmetric scattering at the air–GaAs interface increases the in-coupling efficiency onto the high-index substrate, while light is symmetrically scattered at the air–air interface. The cross section of forward scattering is 5 times higher than that of the backward scattering.

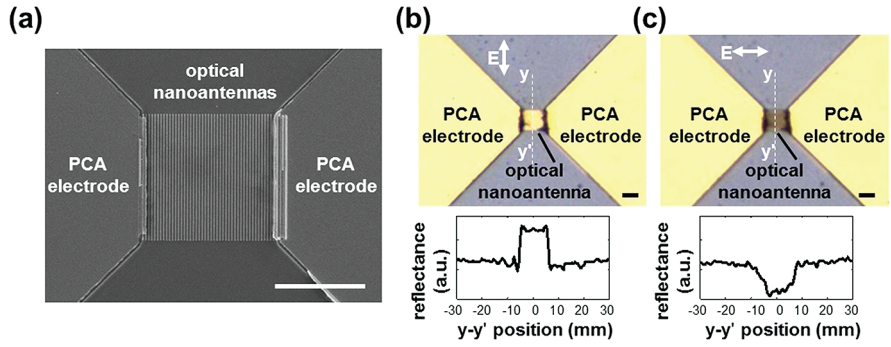

Figure 2. SEM and optical image of the nanoplasmonic PCA (NP-PCA). (a) SEM image of the photoconductive region. Nanorod-type optical nanoantennas are fully integrated between two electrodes of PCA. (b) Parallel-polarized image of the NP-PCA and reflection profile. (c) Perpendicular-polarized image of the NP-PCA and reflection profile. Under a linearly polarized light perpendicular to the longitudinal direction of nanorod arrays, the reflection over a photoconductive region decreases due to high in-coupling efficiency by optical nanoantennas, clearly distinct from a parallel-polarized light. Scale bar is 10 μm in all images.

photoconductive substrate, semi-insulating gallium arsenide (SI-GaAs), as illustrated in Figure 1a. The nanorod-type optical nanoantennas increase the transient photocurrent for high-power THz emission by concentrating and confining an incident ultrashort pulsed optical beam on the high-index photoconductive layer. On the basis of a finite-difference time domain (FDTD) method, two main reasons can be explained as follows: First, the optical antennas locally concentrate an incident optical beam at a plasmon resonance near and between the optical nanoantennas (Figure 1b). Second, the optical antennas also confine the optical beam onto a high-index substrate due to the asymmetric scattering (Figure 1c). Both results contribute to the increase of photocurrent inside the photoconductive layer for high-power THz emission.

In the experiment, the optical nanoantennas were integrated on the interstitial microgap of a bowtie-type PCA on SI-GaAs by incorporating conventional photolithography, electron-beam lithography, and metal lift-off (Figure 2a). The nano- and microfabrication procedures of NP-PCA are as follows: First, a high-resolution electron-beam resist for e-beam lithography was spin-coated and soft-baked on a SI-GaAs substrate after acetone cleaning. The e-beam resist was then developed using 1:3 MIBK/IPA (methyl isobutyl ketone/isopropyl alcohol) after e-beam scanning (ELS-7000, ELIONIX).

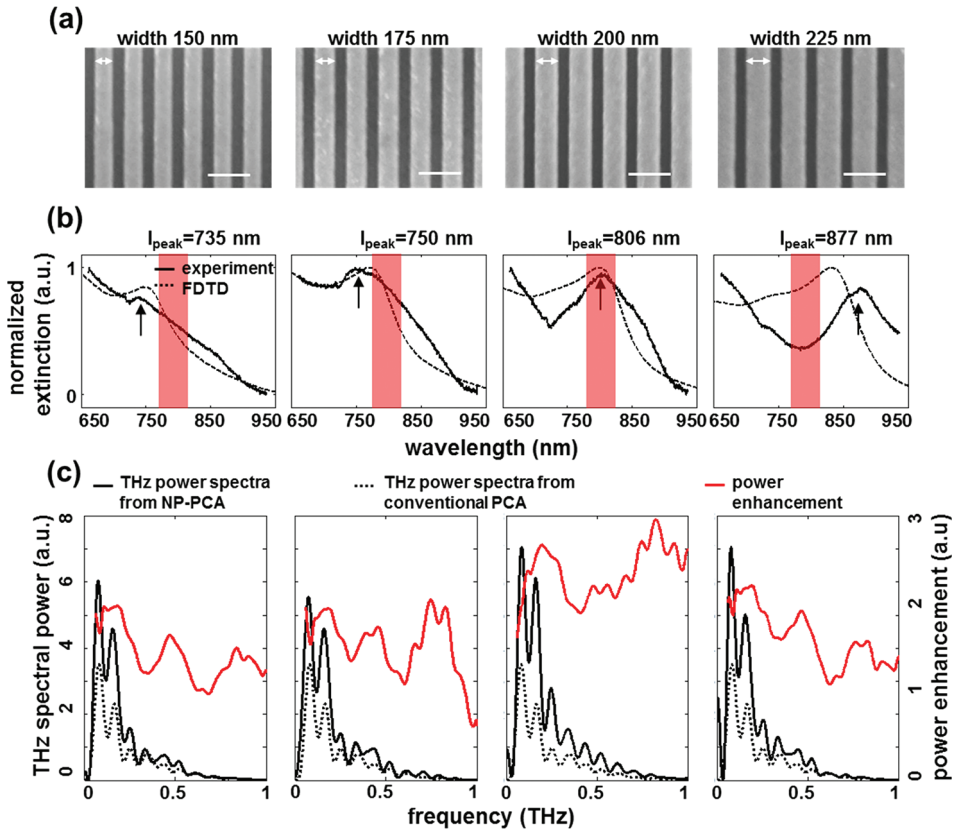

Figure 3. Enhancement of THz emission power by matching the plasmon resonance of optical nanoantennas. (a) SEM images of nanorod-type optical nanoantennas with different widths of 150, 175, 200, and 225 nm. The gap and the thickness are 200 and 50 nm, respectively. The scale bar is 500 nm. (b) Measured (solid line) and calculated (dotted line) extinction spectra of optical nanoantennas (line) with different widths. The measured LSPR peaks are shown at wavelengths of 735, 750, 806, and 877 nm corresponding with the nanorod widths of 150, 175, 200, and 225 nm, respectively. The 200 nm wide nanorod antennas show the plasmon resonance near the center wavelength of an incident ultrashort pulsed beam (800 nm, red shadow). (c) THz power spectra from the NP-PCAs (black line) and a conventional PCA (black dashed line) and the enhancement factors of THz emission power (red line). The maximum enhancement factor of THz emission power, *i.e.*, 2.4 times on average over the 0.1−1.1 THz range and by 3 times at 0.82 THz, is shown from the NP-PCA of 200 nm wide optical nanoantennas with the plasmon resonance near the center wavelength of an incident pump beam, where THz emission power is enhanced by high photocarrier generation in the photoconductive layer.

A 500 Å thick gold film was deposited with a thin chrome adhesion layer by e-beam evaporation, and a metal lift-off process was then performed with acetone. Next, the PCA microelectrodes with a bowtie shape (15 μm wide electrode gap, 90° apex angle) were defined by conventional photolithography under the precise alignment with nanoantennas. Finally, 20 nm thick chrome and 60 nm thick gold films were lifted off with acetone after e-beam evaporation. All of the nano- and microfabrication techniques were done at wafer level. The SEM image shows the fabricated NP-PCA (Figure 2a). The optical nanoantennas are precisely aligned on the 15 μm wide photoconductive region to provide electrical protection against short circuits. The plasmon resonance of the nanorod-type antennas is very sensitive to the polarization of incident light. Under a parallel-polarized incident beam, the reflection of optical nanoantennas is higher than that of a bare SI-GaAs substrate (Figure 2b). However, the reflection under a perpendicular-polarized beam is significantly decreased due to the increase of in-coupling efficiency onto a photoconductive layer of SI-GaAs (Figure 2c).

RESULTS AND DISCUSSION

The enhancement of THz emission power by the optical nanoantennas was experimentally demonstrated by tuning the plasmon resonance with the geometry of nanoantennas. The plasmon resonance can be precisely controlled by changing the nanoantenna width. In this experiment, the nanorod-type optical nanoantennas with four different LSPRs near the excitation wavelength of 800 nm were prepared with PCAs on a SI-GaAs substrate (Figure 3a). The normalized extinction spectra of optical nanoantennas were calculated by a FDTD method and also measured with a reflection microspectrometer under white light illumination by taking $-\log(1 - R)$, where R is the reflectance of NP-PCA. For a constant 50 nm thickness and 200 nm gap, the nanorod arrays with different widths of 150, 175, 200, and 225 nm show the measured LSPR wavelengths at 735, 750, 806, and 877 nm,

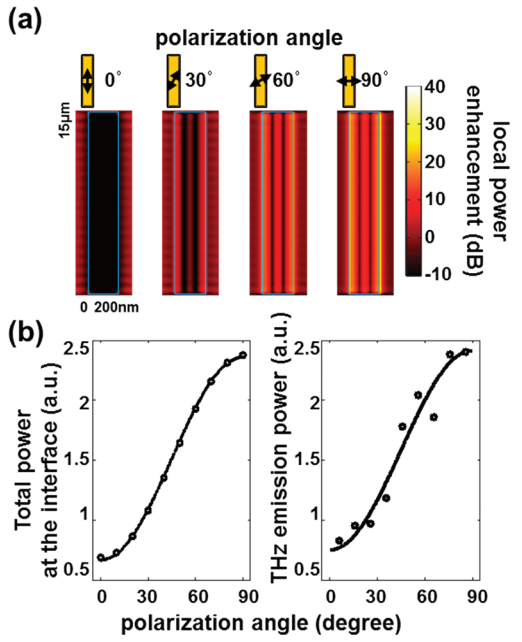

Figure 4. THz emission from the NP-PCA depending on the polarization angle of optical pump beam. (a) Local power enhancement is strongly sensitive to light polarization at the interface between nanorod arrays and the photoconductive substrate. The maximum light concentration by LSPR occurs in the lateral direction under a linearly polarized light perpendicular to the longitudinal direction of nanorod arrays. (b) Total optical power at the interface and THz emission power depending on the polarization angle of incident light. The THz emission power shows the maximum value where total optical power at the interface is maximized, that is, where the polarization of an ultrashort pulsed beam is perpendicularly aligned to the longitudinal direction of nanorod arrays.

respectively (Figure 3b). As the nanorod width increases, both the calculated (dotted line) and the measured (solid line) extinction spectra are clearly red-shifted (Figure 3b) due to the low aspect ratio of the nanorod thickness to the width. Note that the 200 nm wide optical nanoantennas show the LSPR peak near the center wavelength of an incident ultrashort pulsed optical beam (800 nm, red shadow).

The power spectra of THz emission from the four PCAs with different optical nanoantennas were measured by an electro-optical sampling method with an optical pump beam power of 60 mW (Figure 3c).[29] In this measurement, a silicon lens was not mounted on the back side of PCAs to eliminate the variance of THz emission due to a misalignment between the lens and the PCA.[30] The spectral enhancement factor of THz emission power was determined by dividing the THz emission power spectra from NP-PCAs by those from a conventional PCA. All of the NP-PCAs were fabricated on the same wafer to minimize the measurement error. The results show that the enhancement factors in the bandwidth of 0.1−1.1 THz ranges increase as the LSPR peak of optical nanoantennas approaches the center wavelength of an optical pump beam at 800 nm. The PCA with 200 nm wide optical nanoantennas shows the maximum THz emission power due to the LSPR matching. The measured maximum THz power is enhanced by 2.4 times on average over the 0.1−1.1 THz range and by 3 times at 0.82 THz. Furthermore, the THz enhancement factor by 225 nm wide optical nanoantennas is higher than that by 150 and 175 nm wide optical nanoantennas due to high scattering cross section. The scattering cross section increases with the nanoantennas width (see Supporting Information Figure S1). However, the increase of scattering cross section at off-resonance contributes to the small portion of THz emission enhancement. As a result, THz enhancement of NP-PCA is mainly due to the light concentration by matching plasmon resonance and partially due to the light confinement by asymmetric scattering. In addition, the increase of photocurrent within the photoconductive region was calculated in the different depth of a SI-GaAs substrate. The calculated results show that the increase of photocurrent due to light concentration near the optical nanoantennas (~20 nm in depth) accounts for 73% of total photocurrent within the photoconductive volume. It also explains that the increased photocurrent near the optical nanoantennas by light concentration mainly contributes to the THz enhancement. The numerical result also shows that the calculated photocurrent is increased by 2-fold in the photoconductive region under an assumption that the thickness of the photoconductive layer is 110 nm, where the bias electric field falls to 1/*e* of the peak value (see Figure S2 and calculation of photocurrent in Supporting Information). The increase of photocurrent corresponds to a 4-fold THz enhancement factor, which is higher than the measured result. The main difference might originate from the saturation of photocarrier generation. THz emission power from the NP-PCA is saturated around 80 mW, while that from the conventional PCA is increased almost linearly up to 120 mW (Figure S3). Locally enhanced optical power near nanoantennas induces an early saturation of the photocarrier generation and finally saturates the THz emission. As the optical pump beam power is decreased, the enhancement factor approaches the numerical result due to the reduction of photocarrier saturation in the photoconductive layer. The early saturation also implies the enhancement of THz emission by light concentration. On the other hand, no significant loss of the bandwidth is observed. In other words, the change in THz pulse width is negligible in the time domain because the plasmon lifetime of gold is sufficiently short (~10 fs) compared to the pulse width of emitted THz waves (~1 ps).[31]

The THz emission power from the NP-PCA substantially depends on the polarization angle of the optical pump beam due to the polarization sensitivity of nanorod-type optical nanoantenna. The FDTD results show that the local optical power near optical

nanoantennas increases with the polarization angle of the optical pump beam at the interface between nanorod arrays and SI-GaAs (Figure 4a). Under a linearly polarized light perpendicular to the longitudinal direction of nanorods (*i.e.*, 90° polarization angle), the optical nanoantennas clearly exhibit plasmon oscillation in the transverse direction, and the optical power is locally concentrated along both sides of the nanoantenna width. The total optical power is enhanced by 2.4-fold at the interface. In contrast, light concentration is rarely observed under the linear polarization parallel to the longitudinal direction of nanorods due to the nanoantenna length being much longer than a wavelength ($\sim 18\lambda$). The total optical power significantly increases with the polarization angle of the optical pump beam at the interface (Figure 4b), and THz emission power finally increases with the total optical power at the interface (Figure 4c).

The optical nanoantenna for THz enhancement has some unique features compared to conventional anti-reflection coating. First, the optical nanoantenna has higher design flexibility besides anti-reflection coating. For example, the optical nanoantenna can be designed with diverse shapes with different thickness, width, length, or gap to control the field distribution and frequency response, while the design of anti-reflection coating is only limited to optical thickness at the interference condition. Second, the optical nanoantenna increases the photon interaction time for higher photocarrier generation. The optical nanoantenna serves as a scattering element, which results in increasing the optical path length within the photoconductive region. Photon-to-electron conversion is proportional to the interaction time between photon and semiconductor. Besides, a typical plasmon lifetime for gold nanostructures ranges ~10 fs, which results in increasing the conversion rate near plasmonic nanoantennas. Note that a photon typically takes 0.2 fs to travel through the 20 nm depth. Not only two unique features, the optical nanoantenna provides many other opportunities for polarization sensitivity or active plasmonic control. Finally, the optical nanoantenna can additionally enhance THz emission power by localizing optical power within the photoconductive region in addition to the THz enhancement by anti-reflection coating due to the different working principles.

CONCLUSION

In summary, this work demonstrates the enhancement of THz emission power by employing optical nanoantennas with a THz photoconductive antenna. The optical nanoantennas increase the light concentration near gold nanorod arrays at localized surface plasmon resonance and the light confinement in a photoconductive region. As a result, higher photocarrier generation substantially contributes to the increase of THz emission power. The high-power THz emission with optical nanoantennas can be implemented by using large-area excitation, that is, low intensity, with multiple interdigitized microelectrodes under the restricted optical power. This work opens up new possibilities for merging diverse photonic devices at THz and optical frequencies on a single PCA; that is, not only for this particular example but miscellaneous optical nanoantennas can also be employed with conventional PCAs for advanced THz photonics.

METHODS

Measurement of THz Pulse Emission. THz time domain waveforms were measured by an electro-optical sampling method. Ti:sapphire femtosecond pulsed beam with a center wavelength at 800 nm was split for an optical pump and probe beam. The repetition rate was 100 MHz with 10 fs pulse width. This optical beam was focused onto the NP-PCA through a lens under normal incidence. The PCAs were electrically modulated with a 68 kHz, 11 V square-wave voltage for phase modulation measurement. The emitted THz pulses from the NP-PCAs were collected by two parabolic mirrors and focused on a crystal of 1 mm thick (110) ZnTe. The NP-PCA mounted on a 1 in. printed circuit board was aligned with the optical pump beam, where the resistance of the NP-PCA was minimized under illumination.

Conflict of Interest: The authors declare no competing financial interest.

Acknowledgment. This work was supported by the IT R&D program of MKE/KEIT [KI001889, Development of high speed terahertz/NIR spectroscopic endoscopy using THz frequency comb technology] and the National Research Foundation of Korea (NRF) grant funded by Korea government (MEST) (2011-0016481, 2011-0020186, 2011-0031868).

Supporting Information Available: Details of asymmetric scattering profile with different width, the numerical analysis for the bias electric field, calculation of photocurrent and saturation of THz emission power. This material is available free of charge *via* the Internet at http://pubs.acs.org.

REFERENCES AND NOTES

1. Ferguson, B.; Zhang, X. C. Materials for Terahertz Science and Technology. *Nat. Mater.* **2002**, *1*, 26–33.
2. Yen, T. J.; Padilla, W. J.; Fang, N.; Vier, D. C.; Smith, D. R.; Pendry, J. B.; Basov, D. N.; Zhang, X. Terahertz Magnetic Response from Artificial Materials. *Science* **2004**, *303*, 1494–1496.
3. Wang, K. L.; Mittleman, D. M. Metal Wires for Terahertz Wave Guiding. *Nature* **2004**, *432*, 376–379.
4. Chen, H. T.; Padilla, W. J.; Zide, J. M. O.; Gossard, A. C.; Taylor, A. J.; Averitt, R. D. Active Terahertz Metamaterial Devices. *Nature* **2006**, *444*, 597–600.
5. Tonouchi, M. Cutting-Edge Terahertz Technology. *Nat. Photonics* **2007**, *1*, 97–105.
6. Kawase, K.; Ogawa, Y.; Watanabe, Y.; Inoue, H. Non-destructive Terahertz Imaging of Illicit Drugs Using Spectral Fingerprints. *Opt. Express* **2003**, *11*, 2549–2554.

7. Taday, P. F.; Bradley, I. V.; Arnone, D. D.; Pepper, M. Using Terahertz Pulse Spectroscopy To Study the Crystalline Structure of a Drug: A Case Study of the Polymorphs of Ranitidine Hydrochloride. *J. Pharm. Sci.* **2003**, *92*, 831–838.
8. Woodward, R. M.; Cole, B. E.; Wallace, V. P.; Pye, R. J.; Arnone, D. D.; Linfield, E. H.; Pepper, M. Terahertz Pulse Imaging in Reflection Geometry of Human Skin Cancer and Skin Tissue. *Phys. Med. Biol.* **2002**, *47*, 3853–3863.
9. Woodward, R. M.; Wallace, V. P.; Arnone, D. D.; Linfield, E. H.; Pepper, M. Terahertz Pulsed Imaging of Skin Cancer in the Time and Frequency Domain. *J. Biol. Phys.* **2003**, *29*, 257–261.
10. Tani, M.; Herrmann, M.; Sakai, K. Generation and Detection of Terahertz Pulsed Radiation with Photoconductive Antennas and Its Application to Imaging. *Meas. Sci. Technol.* **2002**, *13*, 1739–1745.
11. Dreyhaupt, A.; Winnerl, S.; Dekorsy, T.; Helm, M. High-Intensity Terahertz Radiation from a Microstructured Large-Area Photoconductor. *Appl. Phys. Lett.* **2005**, *86*, 121114.
12. Matthaus, G.; Nolte, S.; Hohmuth, R.; Voitsch, M.; Richter, W.; Pradarutti, B.; Riehemann, S.; Notni, G.; Tunnermann, A. Microlens Coupled Interdigital Photoconductive Switch. *Appl. Phys. Lett.* **2008**, 93.
13. Pradarutti, B.; Muller, R.; Freese, W.; Matthaus, G.; Riehemann, S.; Notni, G.; Nolte, S.; Tunnermann, A. Terahertz Line Detection by a Microlens Array Coupled Photoconductive Antenna Array. *Opt. Express* **2008**, *16*, 18443–18450.
14. Yoneda, H.; Tokuyama, K.; Ueda, K.; Yamamoto, H.; Baba, K. High-Power Terahertz Radiation Emitter with a Diamond Photoconductive Switch Array. *Appl. Opt.* **2001**, *40*, 6733–6736.
15. Catchpole, K. R.; Polman, A. Plasmonic Solar Cells. *Opt. Express* **2008**, *16*, 21793–21800.
16. Schuller, J. A.; Barnard, E. S.; Cai, W. S.; Jun, Y. C.; White, J. S.; Brongersma, M. L. Plasmonics for Extreme Light Concentration and Manipulation. *Nat. Mater.* **2010**, *9*, 193–204.
17. Dorfmuller, J.; Vogelgesang, R.; Khunsin, W.; Rockstuhl, C.; Etrich, C.; Kern, K. Plasmonic Nanowire Antennas: Experiment, Simulation, and Theory. *Nano Lett.* **2010**, *10*, 3596–3603.
18. Genet, C.; Ebbesen, T. W. Light in Tiny Holes. *Nature* **2007**, *445*, 39–46.
19. Novotny, L.; van Hulst, N. Antennas for Light. *Nat. Photonics* **2011**, *5*, 83–90.
20. Schaadt, D. M.; Feng, B.; Yu, E. T. Enhanced Semiconductor Optical Absorption *via* Surface Plasmon Excitation in Metal Nanoparticles. *Appl. Phys. Lett.* **2005**, *86*, 063106.
21. Tang, L.; Kocabas, S. E.; Latif, S.; Okyay, A. K.; Ly-Gagnon, D. S.; Saraswat, K. C.; Miller, D. A. B. Nanometre-Scale Germanium Photodetector Enhanced by a Near-Infrared Dipole Antenna. *Nat. Photonics* **2008**, *2*, 226–229.
22. Shackleford, J. A.; Grote, R.; Currie, M.; Spanier, J. E.; Nabet, B. Integrated Plasmonic Lens Photodetector. *Appl. Phys. Lett.* **2009**, *94*, 083501.
23. Okamoto, K.; Niki, I.; Shvartser, A.; Narukawa, Y.; Mukai, T.; Scherer, A. Surface-Plasmon-Enhanced Light Emitters Based on InGaN Quantum Wells. *Nat. Mater.* **2004**, *3*, 601–605.
24. Ishi, T.; Fujikata, J.; Makita, K.; Baba, T.; Ohashi, K. Si Nano-Photodiode with a Surface Plasmon Antenna. *Jpn. J. Appl. Phys. 2* **2005**, *44*, L364–L366.
25. Pala, R. A.; White, J.; Barnard, E.; Liu, J.; Brongersma, M. L. Design of Plasmonic Thin-Film Solar Cells with Broadband Absorption Enhancements. *Adv. Mater.* **2009**, *21*, 3504–3509.
26. Nakayama, K.; Tanabe, K.; Atwater, H. A. Plasmonic Nanoparticle Enhanced Light Absorption in GaAs Solar Cells. *Appl. Phys. Lett.* **2008**, *93*, 121904.
27. Atwater, H. A.; Polman, A. Plasmonics for Improved Photovoltaic Devices. *Nat. Mater.* **2010**, *9*, 205–213.
28. Munday, J. N.; Atwater, H. A. Large Integrated Absorption Enhancement in Plasmonic Solar Cells by Combining Metallic Gratings and Antireflection Coatings. *Nano Lett.* **2011**, *11*, 2195–2201.
29. Wu, Q.; Zhang, X. C. Free-Space Electrooptic Sampling of Terahertz Beams. *Appl. Phys. Lett.* **1995**, *67*, 3523–3525.
30. Van Rudd, J.; Mittleman, D. M. Influence of Substrate-Lens Design in Terahertz Time-Domain Spectroscopy. *J. Opt. Soc. Am. B* **2002**, *19*, 319–329.
31. Stietz, F.; Bosbach, J.; Wenzel, T.; Vartanyan, T.; Goldmann, A.; Trager, F. Decay Times of Surface Plasmon Excitation in Metal Nanoparticles by Persistent Spectral Hole Burning. *Phys. Rev. Lett.* **2000**, *84*, 5644–5647.